



HAL
open science

Common functional networks in the mouse brain revealed by multi-centre resting-state fMRI analysis

Joanes Grandjean, Carola Canella, Cynthia Anckaerts, Gülebru Ayranci, Salma Bougacha, Thomas Bienert, David Buehlmann, Ludovico Coletta, Daniel Gallino, Natalia Gass, et al.

► To cite this version:

Joanes Grandjean, Carola Canella, Cynthia Anckaerts, Gülebru Ayranci, Salma Bougacha, et al.. Common functional networks in the mouse brain revealed by multi-centre resting-state fMRI analysis. NeuroImage, 2020, 205, pp.116278. 10.1016/j.neuroimage.2019.116278 . hal-03447162

HAL Id: hal-03447162

<https://hal.science/hal-03447162>

Submitted on 24 Nov 2021

HAL is a multi-disciplinary open access archive for the deposit and dissemination of scientific research documents, whether they are published or not. The documents may come from teaching and research institutions in France or abroad, or from public or private research centers.

L'archive ouverte pluridisciplinaire **HAL**, est destinée au dépôt et à la diffusion de documents scientifiques de niveau recherche, publiés ou non, émanant des établissements d'enseignement et de recherche français ou étrangers, des laboratoires publics ou privés.



Common functional networks in the mouse brain revealed by multi-centre resting-state fMRI analysis

Joanes Grandjean^{a,*}, Carola Canella^{b,c}, Cynthia Anckaerts^d, Gülebru Ayranci^e,
 Salma Bougacha^{f,g}, Thomas Bienert^{j,aa}, David Buehlmann^h, Ludovico Coletta^{b,c},
 Daniel Gallino^e, Natalia Gassⁱ, Clément M. Garin^{f,g}, Nachiket Abhay Nadkarni^{f,g},
 Neele S. Hübner^{j,aa}, Meltem Karatas^{j,k}, Yuji Komaki^{l,m}, Silke Kreitzⁿ, Francesca Mandino^{a,o},
 Anna E. Mechling^{j,aa}, Chika Sato^p, Katja Sauerⁿ, Disha Shah^{d,q}, Sandra Strobelⁿ,
 Norio Takata^{l,r}, Isabel Wankⁿ, Tong Wu^{s,t,ac,ad}, Noriaki Yahata^p, Ling Yun Yeow^a, Yohan Yee^u,
 Ichio Aoki^p, M. Mallar Chakravarty^{e,af,ag}, Wei-Tang Chang^a, Marc Dhenain^{f,g},
 Dominik von Elverfeldt^{j,aa}, Laura-Adela Harsan^k, Andreas Hessⁿ, Tianzi Jiang^{s,v},
 Georgios A. Keliris^d, Jason P. Lerch^{u,ab}, Andreas Meyer-Lindenberg^w, Hideyuki Okano^{m,x},
 Markus Rudin^{h,z,ae}, Alexander Sartoriusⁱ, Annemie Van der Linden^d, Marleen Verhoye^d,
 Wolfgang Weber-Fahrⁱ, Nicole Wenderoth^{y,ae}, Valerio Zerbi^{y,ae}, Alessandro Gozzi^b

^a Singapore Biomed Imaging Consortium, Agency for Science, Technology and Research, 11 Biopolis Way, 138667, Singapore

^b Functional Neuroimaging Laboratory, Istituto Italiano di Tecnologia, Centre for Neuroscience and Cognitive Systems @ UNITN, 38068, Rovereto, Italy

^c CIMeC, Centre for Mind/Brain Sciences, University of Trento, 38068, Rovereto, Italy

^d Bio-Imaging Lab, University of Antwerp, CDE, Universiteitsplein 1, 2610, Antwerp, Belgium

^e Douglas Mental Health University Institute, McGill University, Montreal, Quebec, Canada

^f Commissariat à l'Énergie Atomique et Aux Énergies Alternatives (CEA), Direction de la Recherche Fondamentale (DRF), Institut François Jacob, MIRCen, Fontenay-aux-roses, France

^g Centre National de la Recherche Scientifique (CNRS), Université Paris-Sud, Université Paris-Saclay UMR 9199, Neurodegenerative Diseases Laboratory, Fontenay-aux-Roses, France

^h Institute for Biomedical Engineering, University and ETH Zürich, Wolfgang-Pauli-Str. 27, 8093, Zürich, Switzerland

ⁱ Department of Neuroimaging, Central Institute of Mental Health, Medical Faculty Mannheim, University of Heidelberg, Mannheim, Germany

^j Department of Radiology, Medical Physics, Medical Center – University of Freiburg, Faculty of Medicine, University of Freiburg, Killianstr. 5a, 79106, Freiburg, Germany

^k The Engineering Science, Computer Science and Imaging Laboratory (ICube), Department of Biophysics and Nuclear Medicine, University of Strasbourg and University Hospital of Strasbourg, 67000, Strasbourg, France

^l Central Institute for Experimental Animals (CIEA), 3-25-12, Tonomachi, Kawasaki, Kanagawa, 210-0821, Japan

^m Department of Physiology, Keio University School of Medicine, 35 Shinanomachi, Shinjuku, Tokyo, 160-8582, Japan

ⁿ Institute of Experimental and Clinical Pharmacology and Toxicology, Friedrich-Alexander University Erlangen-Nürnberg (FAU), Fahrstraße 17, 91054, Erlangen, Germany

^o Faculty of Life Sciences, University of Manchester, Manchester, United Kingdom

^p Functional and Molecular Imaging Team, Department of Molecular Imaging and Theranostics, National Institute of Radiological Sciences, National Institutes for Quantum and Radiological Science and Technology, Anagawa 4-9-1, Inage, Chiba-city, Chiba, 263-8555, Japan

^q Laboratory for the Research of Neurodegenerative Diseases, VIB Center for Brain and Disease Research, KU Leuven, O&N4 Herestraat 49 Box 602, 3000, Leuven, Belgium

^r Department of Neuropsychiatry, Keio University School of Medicine, 35 Shinanomachi, Shinjuku, Tokyo, 160-8582, Japan

^s Queensland Brain Institute, The University of Queensland, Brisbane, Queensland, Australia

^t Centre for Medical Image Computing, Department of Computer Science, & Max Planck University College London Centre for Computational Psychiatry and Ageing Research, University College London, London, UK

^u Hospital for Sick Children and Department of Medical Biophysics, The University of Toronto, Toronto, Ontario, Canada

^v Brainnetome Center & National Laboratory of Pattern Recognition, Institute of Automation, Chinese Academy of Sciences, Beijing, 100190, China

^w Department of Psychiatry and Psychotherapy, Central Institute of Mental Health, Medical Faculty Mannheim, University of Heidelberg, Germany

^x Laboratory for Marmoset Neural Architecture, RIKEN Brain Science Institute, Wako, Saitama, 351-0198, Japan

^y Neural Control of Movement Lab, Department of Health Sciences and Technology, ETH Zürich, Winterthurerstrasse 190, 8057, Zurich, Switzerland

^z Institute of Pharmacology and Toxicology, University of Zürich, Winterthurerstrasse 190, 8057, Zürich, Switzerland

* Corresponding author. Department of Radiology and Nuclear Medicine & Donders Institute for Brain, Cognition, and Behaviour, Donders Institute, Radboud University Medical Centre, Nijmegen, 6525 EZ, the Netherlands.

<https://doi.org/10.1016/j.neuroimage.2019.116278>

Available online 12 October 2019

1053-8119/© 2019 Elsevier Inc. This is an open access article under the CC BY-NC-ND license (<http://creativecommons.org/licenses/by-nc-nd/4.0/>).

^{aa} BrainLinks-BrainTools Cluster of Excellence, University of Freiburg, Georges-Köhler-Allee 80, 79110, Freiburg, Germany

^{ab} Wellcome Centre for Integrative Neuroimaging, University of Oxford, Oxford, OX3 9DU, UK

^{ac} Computational, Cognitive and Clinical Imaging Lab, Division of Brain Sciences, Department of Medicine, Imperial College London, W12 0NN, UK

^{ad} UK DRI Centre for Care Research and Technology, Imperial College London, W12 0NN, UK

^{ae} Neuroscience Center Zürich, ETH Zürich and University of Zürich, Zürich, Switzerland

^{af} Department of Psychiatry, McGill University, Montreal, Quebec, Canada

^{ag} Department of Biological and Biomedical Engineering, McGill University, Montreal, Quebec, Canada

ARTICLE INFO

Keywords:

Functional connectivity

Default-mode network

ICA

Seed-based

Connectome

ABSTRACT

Preclinical applications of resting-state functional magnetic resonance imaging (rsfMRI) offer the possibility to non-invasively probe whole-brain network dynamics and to investigate the determinants of altered network signatures observed in human studies. Mouse rsfMRI has been increasingly adopted by numerous laboratories worldwide. Here we describe a multi-centre comparison of 17 mouse rsfMRI datasets via a common image processing and analysis pipeline. Despite prominent cross-laboratory differences in equipment and imaging procedures, we report the reproducible identification of several large-scale resting-state networks (RSN), including a mouse default-mode network, in the majority of datasets. A combination of factors was associated with enhanced reproducibility in functional connectivity parameter estimation, including animal handling procedures and equipment performance. RSN spatial specificity was enhanced in datasets acquired at higher field strength, with cryoprobes, in ventilated animals, and under medetomidine-isoflurane combination sedation. Our work describes a set of representative RSNs in the mouse brain and highlights key experimental parameters that can critically guide the design and analysis of future rodent rsfMRI investigations.

1. Introduction

The brain is the most complex organ, consisting of 86 billion neurons (Azevedo et al., 2009), each forming on average 7000 synapses. Understanding the complexity of the brain is difficult due to limited access to the tissue and the imperative for minimally invasive procedures in human subjects. Resting-state functional magnetic resonance imaging (rsfMRI) has gained attention within the human neuroimaging community due to the possibility of interrogating multiple resting-state networks (RSNs) with a relatively high spatial and temporal resolution (Biswal et al., 2010, 1995; Fox and Raichle, 2007) in a minimally invasive manner. Functional connectivity (FC), i.e. the statistical association of two or more time-series extracted from spatially defined regions in the brain (Friston, 2011), is the principal parameter estimated from rsfMRI studies. The importance of FC to neuroscience research can be understood through its widespread use to describe functional alterations in psychiatric and neurological disorders (Buckner et al., 2008; Greicius, 2008). However, despite an extensive characterization of the functional endophenotypes associated with diseased states, limitations to invasiveness and terminal experiments generally preclude the establishment of detailed mechanisms in humans, as can be achieved with animal models.

Since its onset in 2011 (Jonckers et al., 2011), mouse rsfMRI methods have been developed in several centres and have grown to become a routine procedure for phenotyping the brain (Chuang and Nasrallah, 2017; Gozzi and Schwarz, 2016; Hoyer et al., 2014; Jonckers et al., 2015, 2013; Pan et al., 2015). Prominently, mouse rsfMRI has been used to investigate an extensive list of models, including Alzheimer's disease (Grandjean et al., 2014b, 2016b; Shah et al., 2013, 2016c; Wiesmann et al., 2016; Zerbi et al., 2014), motor (DeSimone et al., 2016; Li et al., 2017), affective (Grandjean et al., 2016a), autism spectrum (Bertero et al., 2018; Haberl et al., 2015; Liska et al., 2018; Liska and Gozzi, 2016; Michetti et al., 2017; Sforazzini et al., 2016; Zerbi et al., 2018; Zhan et al., 2014), schizophrenia (Errico et al., 2015; Gass et al., 2016), pain (Buehlmann et al., 2018; Komaki et al., 2016), reward (Charbogne et al., 2017; Mechling et al., 2016), and demyelinating disorders (Hübner et al., 2017). Another application of mouse rsfMRI is the elucidation of large-scale functional alterations exerted by pharmacological agents (Razoux et al., 2013; Shah et al., 2016a, 2015). Finally, the method has been used to address fundamental questions. These include the investigation of the structural basis underlying FC (Bergmann et al., 2016; Grandjean et al., 2017b; Hübner et al., 2017; Schroeter et al., 2017; Sforazzini et al., 2016; Stafford et al., 2014), the nature of the dynamical

event encoded in the resting-state signal (Belloy et al., 2018a, 2018b; Bukhari et al., 2018; Grandjean et al., 2017a; Gutierrez-Barragan et al., 2019; Sethi et al., 2017), as well as strain (Jonckers et al., 2011; Schroeter et al., 2017; Shah et al., 2016b), and the impact of sedation or awake conditions on the underlying signal and connectivity patterns (Bukhari et al., 2017; Grandjean et al., 2014a; Jonckers et al., 2014; Wu et al., 2017; Yoshida et al., 2016). This body of work obtained mainly over the past 5 years reflects the growth and interest in this modality as a translational tool to understand the mechanisms underlying the organisation of RSNs in healthy and diseased states, with the promise of highlighting relevant targets in the drug development process and advancing fundamental knowledge in neuroscience.

Despite a growing interest in the field, rsfMRI studies in animals have been inherently difficult to compare. On top of centre-related confounds analogous to those observed in human studies (Jovicich et al., 2016), comparisons in rodents are further confounded by greater variability in preclinical equipment (e.g. field strength, hardware design), animal handling protocols, and sedation regimens employed to control for motion and stress. Discrepancies between reports, such as the anatomical and spatial extent of a rodent homologue of the human default-mode network (DMN) (Becerra et al., 2011; Gozzi and Schwarz, 2016; Guilfoyle et al., 2013; Hübner et al., 2017; Liska et al., 2015; Lu et al., 2012; Sforazzini et al., 2014; Stafford et al., 2014; Upadhyay et al., 2011), or the organisation of murine RSNs (Jonckers et al., 2011), have stark consequences for the interpretation of the results.

To establish standards and points of comparison in rodent fMRI, a growing need in the field, we carried out a multi-centre comparison of mouse rsfMRI datasets. Datasets representative of local centre acquisitions were analysed with a common pre-processing pipeline and examined with seed-based analyses (SBA) and independent component analyses (ICA), two common brain mapping methods used to investigate RSNs. Our work aims to identify representative mouse RSNs, to establish a set of reference pre-processing and analytical steps, and to highlight protocols associated with more sensitive and specific FC detection in the mouse brain.

2. Material and methods

2.1. Resting-state fMRI acquisition

All animal experiments were carried out with explicit permits from local regulatory bodies. Seventeen datasets, consisting of 15 individual

pre-acquired rsfMRI scans each, were acquired with parameters reflecting each centre's standard. A dataset is defined here as a collection of scans acquired under one protocol by one group of individuals on a specific piece of equipment. A scan is a single rsfMRI acquisition obtained from an individual mouse. A summary of the equipment, acquisition parameters, and animal handling procedures are listed in [Supplementary Table 1](#). Scans were acquired on dedicated Bruker magnets operating at 4.7 T (N = 1 dataset), 7 T (N = 8), 9.4 T (N = 6), or 11.7 T (N = 2), with either room-temperature coils (N = 7) or cryoprobes (N = 10). Gradient-echo echo planar imaging (EPI) sequences were used to acquire all datasets, with repetition time (TR) ranging from 1000 ms to 2000 ms, echo time (TE) from 10 to 25 ms, and number of volumes from 150 to 1000. Acquisitions were performed on awake (N = 1) or anaesthetized C57Bl/6 J mice (both male and female) with either isoflurane 1–1.25% (N = 5), halothane 0.75% (N = 1), medetomidine 0.1–0.4 mg/kg bolus and 0.2–0.8 mg/kg/h infusion (N = 5), or a combination of isoflurane 0.2–0.5% and medetomidine 0.05–0.3 mg/kg bolus and 0–0.1 mg/kg/h infusion (N = 5). Awake mice were fitted with a non-magnetic head implant to fix their heads to a compatible cradle ([Yoshida et al., 2016](#)). Animals were either freely-breathing (N = 12) or mechanically ventilated (N = 5). Datasets are publicly available in the BIDS format on openneuro.org (project ID: Mouse_rest_multicentre, [10.18112/openneuro.ds001720.v1.0.2](https://openneuro.org/ds001720.v1.0.2)).

2.2. Data pre-processing

Volumes were analysed in their native resolution. First, image axes were reoriented into LPI orientation (*3dresample*, Analysis of Functional NeuroImages, AFNI_16.1.26, <https://afni.nimh.nih.gov>) ([Cox, 1996](#)). Temporal spikes were removed (*3dDespike*), followed by motion correction (*3dvolreg*). Brain masks (*RATS_MM*, <https://www.iibi.uiowa.edu>) ([Oguz et al., 2014](#)) were estimated on temporally averaged EPI volume (*fslmaths*). Motion outliers were detected based on relative framewise displacement (FWD) estimated during motion correction. Volumes with spikes or FWD greater than 0.1 mm, corresponding to approximately 0.5 voxel of the average in-plane resolution, were labelled in a confound file to be excluded from later seed-based and dual-regression analyses. Linear affine parameters and nonlinear deformations with greedy SyN diffeomorphic transformation (*antsIntroduction.sh*) were estimated relative to a reference T2 MRI template ([Dorr et al., 2008](#)) registered to the Allen Institute for Brain Science (AIBS) Common Coordinate Framework space (CCF v3, © 2004 Allen Institute for Brain Science. Allen Mouse Brain Atlas. Available from: <http://www.brain-map.org/>) ([Lein et al., 2007](#)) and resampled to $0.2 \times 0.2 \times 0.2 \text{ mm}^3$. The normalisation to AIBS space was carried out on brain-masked EPI using ANTS (Advanced Normalisation Tools, <http://picsl.upenn.edu/software/ants/>) ([Avants et al., 2014, 2011](#)). Anatomical scans corresponding to each EPI acquisition were not available in all cases. Despite this limitation, plausible registrations of EPI directly to a T2 MRI template were rendered possible due to the relatively simple structure of the lissencephalic cerebrum and high EPI quality. Individually registered brain masks were multiplied (*fslmaths*) to obtain a study mask. The analyses were performed within this study mask, i.e. within the brain areas covered by all individual scans. References to anatomical areas are made with respect to the AIBS atlas. All brain masks and registrations were visually inspected and considered plausible.

Six different denoising approaches were applied: i) 6 motion parameters regression (MC), or the following together with motion parameters, ii) white matter (WM), iii) ventricle (VEN), iv) vascular (VASC), v) vascular + ventricle (VV), or vi) global (GSR) signal regression. White matter and ventricle masks were adapted from the AIBS atlas ([Supplementary Figure 1c,d](#)). A group-level vascular mask was obtained by combining hand-selected individual-level independent components (threshold $z > 2.3$ corresponding to $p < 0.01$ uncorrected) overlapping with vascular structures ([Supplementary Figs. 1b and 2](#)). These vascular-associated components were identified in a subset of scans supporting the

notion of vascular signal confounds. Inverse transformations were applied to each mask. Average time series within masks were extracted (*fslmeans*) and regressed out (*fslregfilt*). Then, spatial smoothing was applied using an isotropic 0.45 mm kernel (*3dBlurInMask*) corresponding approximately to 1.5 x voxel spacing along the dimension of the lowest resolution. Finally, bandpass filtering (0.01–0.1 Hz) was applied (*3dBandpass*). The bandpass filter was applied to all datasets to enhance comparability between datasets, despite indications that medetomidine leads to a shift in resting fluctuation frequencies ([Grandjean et al., 2014a; Kalthoff et al., 2013; Paasonen et al., 2018](#)). The denoised and filtered individual scans were normalised to AIBS reference space (*WarpTimeSeriesImageMultiTransform*).

The noise was estimated by extracting the signal standard deviation from manually defined regions-of-interest (ROIs) in the upper corners of at least 3 slices, carefully avoiding ghosting artefacts or tissues (brain or otherwise). Mean signal was extracted from the 20th acquisition volume using a cortical mask spanning the whole isocortex (defined by AIBS atlas) and registered in individual spaces to estimate signal-to-noise ratio (SNR). The same cortical mask was used to extract standard deviation of temporal signals to estimate temporal SNR (tSNR).

2.3. Seed-based analysis and independent component analysis

Seeds in the left hemisphere were defined in AIBS space based on the AIBS atlas using 0.3 mm^3 spheres, corresponding to 27 voxels ([Supplementary Fig. 1a](#)). The mean BOLD signal time-series within a seed were extracted (*fslmeans*) and regressed into individual scans to obtain z-statistic maps (*fslglm*). Multi-session temporal concatenation ICA was carried out using MELODIC (Multivariate Exploratory Linear Optimized Decomposition into Independent Components, v3.14) (20 components). The group-level component classification was adapted on a defined set of rules ([Zerbi et al., 2015](#)). The following were considered plausible: (i) components with either bilateral organisation or (ii) unilateral components with a corresponding separate contralateral component, (iii) minimal crossing of relevant brain boundaries such as white matter tracts, (iv) spatial extent covering more than one slice. The following were considered implausible: (i) components overlapping mainly with either white matter, ventricle, or vascular masks ([Supplementary Fig. 1b,c,d](#)), (ii) components mainly localised on brain edges. Dual-regression analysis was carried out using the eponymous FSL function to obtain individual-level representations of 14 selected plausible group-level components ([Filippini et al., 2009](#)).

2.4. Statistical analysis and data representation

Voxelwise statistics were carried out in FSL using either nonparametric permutation tests (*randomise*) for across-dataset comparisons (5000 permutations and voxelwise correction), or uncorrected parametric one-sample t-tests for within-dataset comparisons (*fslglm*). The decision to present within-dataset comparisons using uncorrected parametric statistics is motivated by the desire to mitigate false-negative rates, and hence avoiding to reject potential FC. This is however done at the expense of enhanced false-positive rates. Within-dataset comparisons are summarised as “overlap maps”, i.e. the percentage of overlapping datasets exhibiting significance in one-sample t-tests at a given voxel. To account for the false-positive rates imposed by our significance threshold and for clarity in their representation, overlap maps are presented as overlays with a 30–100% range. For additional clarity, the statistical maps relative to each dataset are detailed in the supplementary materials for one representative SBA. Voxelwise statistical maps are shown as colour-coded t-statistics overlays on the ABI template resampled at $0.025 \times 0.025 \times 0.025 \text{ mm}^3$ using MRICron ([Rorden et al., 2007](#)). Statistical analysis carried out on parameters extracted from ROIs was performed in R (v3.4.4, “Someone to Lean on”, R Foundation for Statistical Computing, Vienna, Austria, <https://R-project.org>) using a linear model (*lm*). A simplified model was designed to include the following

fixed effects: breathing conditions (2 levels: ventilated or free-breathing), sedation conditions (4 levels: awake, isoflurane/halothane, medetomidine, medetomidine + isoflurane combination), SNR (continuous variable), and mean FWD (continuous variable). Interaction effects between these factors were not modelled. Fixed effects' significance were tested using a likelihood ratio test. Scan parameter occurrence rates were assessed with a Chi-square test (*chisq.test*). Residual analyses were also performed; QQ-plots were used to assess normality of distributions, Tukey–Anscombe plots for the homogeneity of the variance and skewness, and scale location plots for homoscedasticity (i.e. the homogeneity of residual variance). The assumptions of normality of the residuals were considered plausible in all statistical tests. Plots were generated using ggplot2 (v2.1.0) package for R. Significance level was set at one-tailed $p \leq 0.05$ with family-wise error correction at a voxelwise level, unless specified otherwise. Descriptive statistics are given as mean \pm 1 standard deviation.

3. Results

3.1. Dataset description and pre-processing validation

A total of 17 datasets, each consisting of 15 individual rsfMRI scans, were included in this study. Dataset selection was restricted to gradient-echo echo planar imaging scans acquired on healthy and wild-type C57Bl/6J mice, any gender, any age, and any sedation protocol (Supplementary Table 1). Cortical SNR ranged from 17.04 to 448.56, while tSNR ranged from 8.11 to 112.68 (Fig. 1a,b). A comparison between SNR and tSNR indicated a positive association between the two measures (Pearson's $r = 0.75$, $t = 18.30$, $df = 253$, $p = 2.2e-16$). Due to the lack of orthogonality between the two factors, only SNR was considered in the remaining analyses. Mean FWD ranged from 0.0025 mm to 0.1500 mm (Fig. 1c). A summary of representative estimated motion parameters is shown in the supplementary material (Supplementary Fig. 3). Each pre-processing output was visually inspected. Automatic brain extraction generated plausible brain masks. Normalisation was carried out using the AIBS template (Supplementary Fig. 4). Spatial coverage along the anterior-posterior axis varied across datasets. The following analysis is thus restricted to areas fully covered by all scans, corresponding to approximately 2.96 and -2.92 mm relative to Bregma. Moreover, distortions made it impossible to cover the amygdala region in full. No marked difference in the performance of each pre-processing step was identified between datasets. The brain-masked, spatially smoothed, temporally filtered, and normalised scans were further processed as follows.

3.2. Vascular and ventricle signal regression enhances functional connectivity specificity

Denoising procedures are an integral step to all FC analyses relying on rsfMRI acquisitions. Nuisance signal originates from multiple sources, including physiological and equipment-related noise (Murphy et al., 2013). No consensus exists both in human and rodent fMRI fields regarding optimal noise removal procedures. In this study, the following six nuisance regression models were designed and compared, with one model selected for the remaining analyses based on objective criteria. The first nuisance model includes only motion parameter regression (MC). Global signal regression (GSR) was added to the motion parameter in a second model. The signal from either white-matter (WM), ventricle (VEN), or vascular (VASC) masks (Supplementary Fig. 1b,c,d) were combined with motion parameters in additional regression models. Finally, based on the results obtained with these approaches, a combination (VV) model including VEN and VASC signal regression was included in the comparison. The effectiveness of nuisance regression models and the specificity of the resulting networks at the subject level were assessed based on the outcome of SBA using the anterior cingulate area (ACA, Supplementary Fig. 1a) as the seed region. This seed was

selected as a central node of the putative rodent DMN (Gozzi and Schwarz, 2016).

The statistical map of a one-sample *t*-test across all (255/255) individual maps following GSR (Fig. 2a) indicated positive FC along the rostral-caudal axis, through the ACA and extending to the retrosplenial area (RSP), with anti-correlations in adjacent primary somatosensory areas (SSp). In the VV nuisance model, as compared to the GSR model, a more extended network was revealed to include posterior parietal cortical areas (Fig. 2b), while anti-correlations in the SSp did not reach statistical significance. To assess the specificity of the obtained functional networks, subject-level FC parameters (z-statistic) were extracted from ROIs located in the RSP and left SSp. The former was defined as a specific ROI, i.e. an ROI where positive FC is expected, while the latter was defined as a non-specific ROI, i.e. an ROI where low or negative FC is expected. The decision to consider these two areas as belonging to separable network systems reflects several lines of converging evidence: a) these regions are not linked by major white matter bundles or direct axonal projections in the mouse brain (Oh et al., 2014), b) they reflect separable electrophysiological signatures in mammals (Popa et al., 2009), and c) they belong to separable functional communities (Liska et al., 2015) in the mouse brain and are similarly characterized by the absence of significant positive correlation in the corresponding human RSN (Fox et al., 2005).

Detailed FC within the specific ROI for the GSR and VV nuisance model are shown as a function of FC within the corresponding non-specific ROI at the single-subject level (Supplementary Fig. 5). In the VV condition, 98/255 (i.e. 38%) of individual scans fell into the "specific FC" category, while both MC and GSR conditions reach the lowest percentage (30%) of scans exhibiting "specific FC" relative to the ACA seed (Fig. 2c). Out of 98/255 scans categorised as presenting "specific FC" relative to the ACA seed, up to 14/15 scans originated from the same dataset (median = 6/15). Two datasets did not contain scans that met the definition. The 98 scans were also unevenly distributed according to the different acquisition parameters, including field strength (4.7 T $N = 1/15$, 7 T $N = 41/120$, 9.4 T $N = 38/90$, 11.7 T $N = 18/30$, $X^2 = 13.76$, $df = 3$, p -value = 0.0032), coil type (room-temperature $N = 26/105$, cryoprobe $N = 72/150$, $X^2 = 13.13$, $df = 1$, p -value = 0.00029), breathing condition (free-breathing $N = 58/180$, ventilated $N = 40/75$, $X^2 = 9.10$, $df = 1$, p -value = 0.0026), and sedation condition (awake $N = 7/15$, isoflurane/halothane $N = 18/90$, medetomidine $N = 26/75$, medetomidine + isoflurane $N = 47/75$, $X^2 = 32.42$, $df = 3$, p -value = 4.28e-07). Hence, scans presenting "specific FC" patterns were more often found in datasets acquired at higher field strengths, with cryoprobes, in ventilated animals, and under medetomidine + isoflurane combination sedation.

To test how FC is affected as a function of distance to the seed and nuisance model, FC in the ACA and RSP along the anterior-posterior axis was extracted (Fig. 2d). Comparable rate of decrease was observed in all conditions, with GSR displaying an overall decrease of FC. This is consistent with the overall decrease in FC induced by GSR relative to VV in the specificity analysis (Supplementary Fig. 5). In summary, the VV nuisance model enhanced the specificity of SBA-derived DMN, as indicated by a higher frequency of scans in the "specific FC" category. Based on this criterion, this nuisance model was used in all subsequent analyses.

3.3. Seed-based analysis identifies common and reproducible mouse resting-state networks

We sought to identify common RSNs by employing SBA and to compare reproducibility across datasets. Seeds positioned in representative anatomical regions of the left hemisphere (Supplementary Fig. 1a) were used to reveal the spatial extent of previously described mouse resting-state networks. The seeds were selected to represent different cortical (somatosensory, motor, high order processing), as well as subcortical systems (striatum, hippocampal formation, thalamus). To obtain high-specificity and high-confidence group-level SBA maps, we

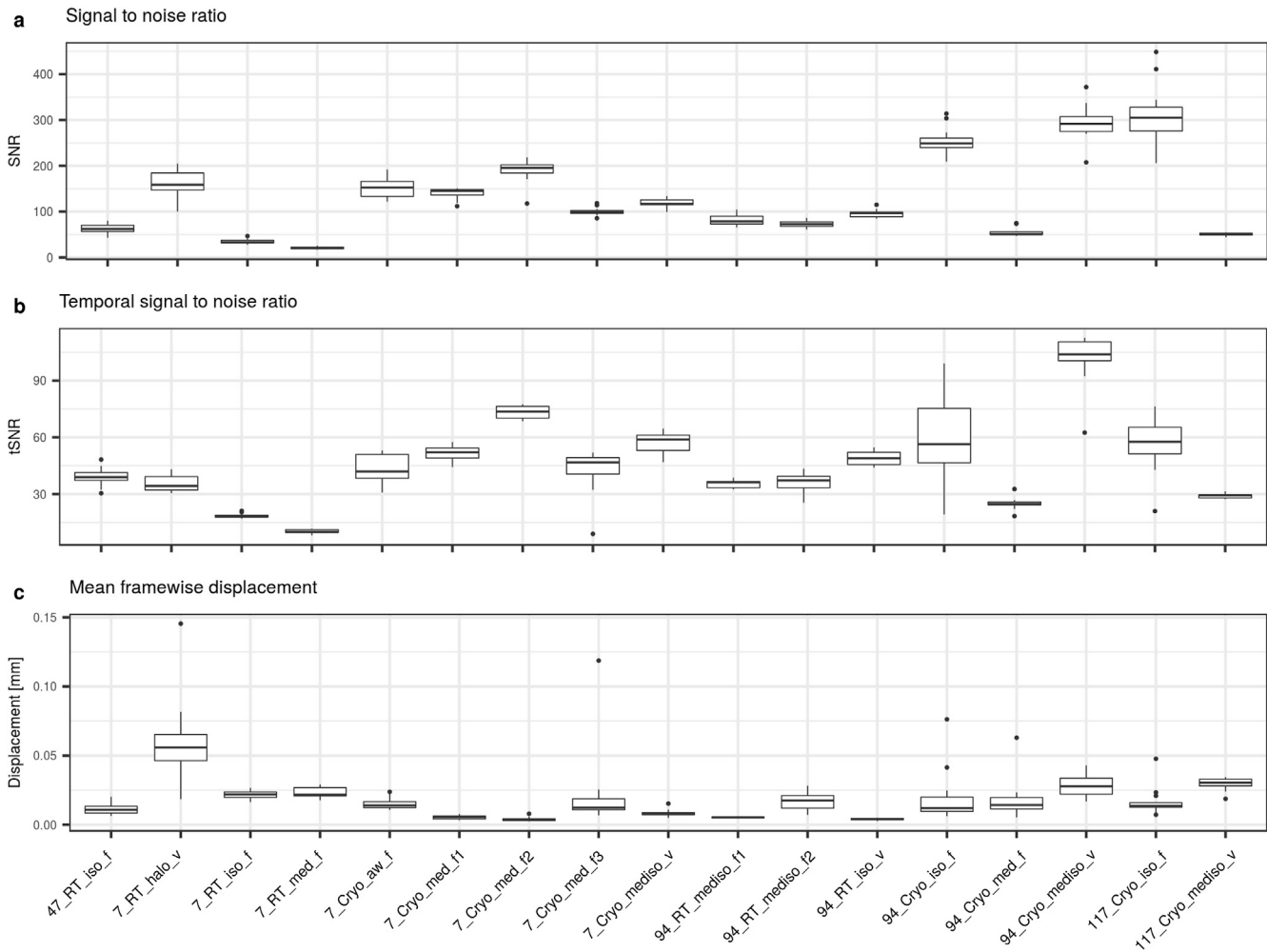


Fig. 1. Dataset description. Signal-to-Noise Ratio (SNR), temporal SNR (tSNR), and mean framewise displacement are presented as a function of dataset. There is a positive association between tSNR and SNR ($r = 0.75$, $t = 18.30$, $df = 253$ $p = 2.2e-16$).

first probed only 98/255 scans listed as containing “specific FC” in the previous analysis. We next extended these analyses to include all 255/255 scans (Supplementary Fig. 7). For the within-dataset comparisons, all 15/15 scans in each dataset were included to reflect inter-dataset variability.

All group-level SBA maps exhibited a strong bilateral and homotopic extension (Fig. 3a, Supplementary Fig. 6). An ACA seed revealed a network involving the prefrontal cortex, RSP, dorsal striatum, dorsal thalamus and peri-hippocampal areas. This recapitulates anatomical features reminiscent of the human, primate, and rat DMN (Gozzi and Schwarz, 2016; Hutchison and Everling, 2012; Sforazzini et al., 2014; Stafford et al., 2014). Comparable regions were observed for the RSP seed, a region evolutionarily related to the posterior cingulate cortex of the human DMN (Supplementary Fig. 6). The anterior insular seed was found to be co-activated with the dorsal cingulate and the amygdalar areas, corresponding to the putative rodent salience network (Gozzi and Schwarz, 2016), while the primary somato-motor region (MO) defined a previously described latero-cortical network that appears to be antagonistic to midline DMN regions. Hence it has been postulated to serve as a possible rodent homologue of the primate task-positive network (Fig. 3a) (Liska et al., 2015; Sforazzini et al., 2014). The corresponding networks estimated across all scans (255/255) recapitulated features identified in the 98/255 scans listed as containing “specific FC” but appeared to have a much lower spatial specificity (Supplementary Fig. 7). Overlap maps summarising the results from each individual dataset revealed that 70% (12/17) of the datasets presented the features listed above (Fig. 3b).

Overlap maps indicate, on a voxel basis, the percentage of the dataset presenting a significant FC following a one-sample *t*-test performed on its 15 scans. The one-sample *t*-test maps relative to each dataset are detailed in Supplementary Fig. 8. They confirmed the different extent of network detection in different datasets. In summary, this analysis revealed the commonly shared spatial extent of mouse RSNs derived from SBA but also indicates that a small subset of the datasets failed to present these features with sufficient sensitivity or specificity.

3.4. Sedation protocol and SNR affect connectivity strength

The datasets analysed here were acquired at varying field strengths, and with different coil designs, EPI sequence parameters, animal handling procedures, and anaesthesia protocols, i.e. either awake or sedated states. Hence the acquisitions were not purposefully balanced to test specific effects. To identify factors associated with FC strength, a simplified linear model was designed including the following explanatory factors: sedation and breathing conditions, SNR, and motion (mean FWD). Limitations in the orthogonality and representation of specific acquisition factors such as field strength, coil design, EPI sequence parameters, number of volumes, gender, and age prevented designing a more extensive model.

Individual-level FC values (z-statistic) were extracted from SBA maps estimated from the ACA seed using an ROI located in the RSP and shown as a function of different acquisition parameters (Fig. 4). Sedation protocol ($F_{(247, 251)} = 18.29$, $p = 3.5e-13$) and SNR ($F_{(247, 248)} = 12.39$,

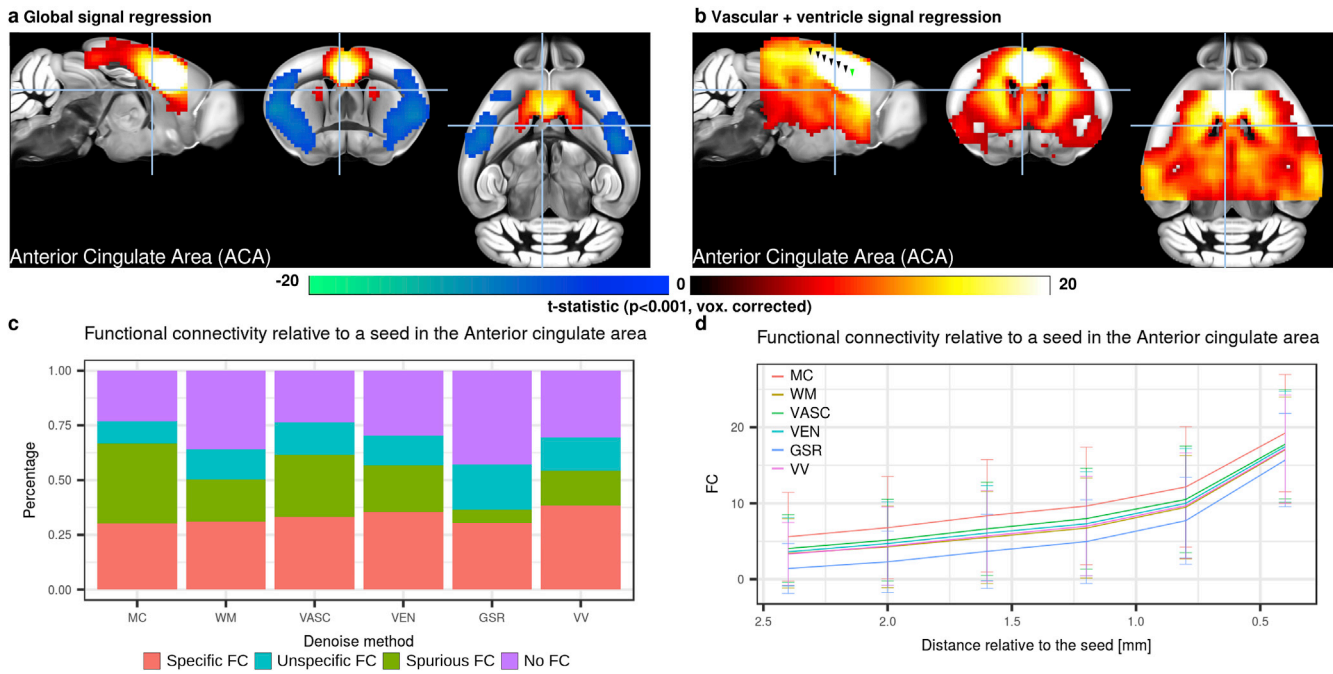


Fig. 2. Denoising strategies and their impact on functional connectivity (FC) specificity. **a-b**, Seed-based analysis for a seed in the anterior cingulate area (ACA) following either global signal regression (GSR, **a**) or vascular + ventricle signal regression (VV, **b**). The spatial maps obtained lead to a set of regions for which the BOLD signals were positively associated with the BOLD signal of the ACA. These included the prefrontal cortex, retrosplenial area (RSP), and dorsal striatum. Under VV, the connectivity profile extended to peri-hippocampal areas. Significant anti-correlation (negative t-statistic, blue) are also present in the primary somatosensory areas (SSp) under GSR but not VV condition. Individual scans were classified as presenting “Specific”, “Unspecific”, “Spurious”, or “No” FC relative to the ACA seed (**c**, see [Supplementary Fig. 5](#) for details). Comparison of each FC category depending on the denoising strategies revealed that motion correction and GSR lead to the lowest percentage of “specific FC” at 30%, while that percentage was highest under VV condition (38%). FC as a function of distance to the ACA seed indicates a comparable rate of decline between denoising strategies (**d**). Green arrowhead indicates the position of the ACA seed, black arrowheads indicate ROIs spaced 0.4 mm apart, shown in panel **b**. Voxelwise corrected t-statistics for one-sample t-tests ($p < 0.001$, corrected) are shown as colour-coded overlays on the AIBS reference template. Descriptive statistics are shown as mean \pm 1 standard deviation.

$p = 5.1 \times 10^{-4}$) were significantly associated with FC, while the remaining factors, breathing condition ($F_{(247, 248)} = 3.48$, $p = 0.063$) and motion ($F_{(247, 248)} = 0.082$, $p = 0.77$) were not. The awake and medetomidine + isoflurane combination led to higher FC compared to the other two sedation categories. Concerning SNR, high FC values started to be observed at $SNR > 50$, suggesting that lower SNR may not be sufficient to detect relevant fluctuations. Interestingly, these effects were found to be consistent across the different ROI pairs ([Supplementary Table 1](#)), thus confirming the importance of sedation conditions and SNR, and suggesting that breathing conditions mildly impact FC sensitivity.

The animal handling conditions and sedation protocols highlighted here may not apply to all studies or laboratories due to local legislation, equipment availability, or technical knowledge. Distributions of FC values may hence provide useful reference points. Connectivity strength between the ACA and RSP, representing a central feature of the rodent DMN, reached $z = 2.77$, 5.71, and 10.46 at the 50th, 75th, and 95th percentile respectively (Pearson’s $r = 0.15$, 0.26, 0.43, when SBA is carried out using a correlation analysis instead of a general linear model). Additional SBA parameter distributions are provided for other ROI pairs in [Supplementary Table 1](#). The parameters of the acquisitions featured in this analysis offer an objective criterion to evaluate and compare sensitivity to FC in a new dataset or previous publications, insofar as comparable metrics are available.

3.5. Network-specific functional connectivity is found in all datasets

Evidence for robust distal FC could not be established in all datasets with SBA. To investigate the presence of network-specific FC also in datasets characterized by weaker distal connectivity, a dual regression combined with group-level ICA (driICA) approach was performed

([Filippini et al., 2009](#)). To obtain an enriched data-driven reference atlas, a group ICA atlas was generated out of the 98 “specific FC” scans selected in the SBA above, using 20 dimensions. This was motivated by the observation of spurious FC in one-sample t-test of SBA maps when all scans were included ([Fig. 2b](#)). The atlas revealed 9 cortical components ([Fig. 5a](#), [Supplementary Fig. 9](#), [Supplementary Table 3](#)), 5 overlapping with the latero-cortical network (MO and 4 SSp areas), 3 overlapping with elements of the DMN (prefrontal, cingulate/RSP, and temporal associative areas), and 1 overlapping with the insular area (AI). Additionally, 5 sub-cortical components were revealed, overlapping with the nucleus accumbens (ACB), caudoputamen (CP), pallidum (PAL), hippocampal region (HIP), and thalamus (TH) ([Supplementary Fig. 10](#)). The components recapitulate many of the features identified with SBA ([Fig. 5b](#) and **c**), namely a homotopic bilateral organisation. The components identified here also presented strong similarities to a previous analysis ([Zerbi et al., 2015](#)). Due to uneven brain coverages across datasets, rostral and caudal RSNs could not be examined, including olfactory, auditory, and visual networks. To obtain individual-level representations of these components, a dual regression approach was implemented using the reference ICA identified above. These group-level ICA were used as masks to extract time series which were then regressed into all (255/255) individual scans using a general linear model. To investigate specificity relative to a DMN-related component, FC relative to the cingulate/RSP component was extracted from the ACA ROI (Specific ROI, $z = 9.68$, 16.28, and 24.24, 50th, 75th, and 95th percentiles, [Fig. 5e](#)) and SSp ROI (Unspecific ROI). “Specific FC” was determined in 79% (201/255) of the scans, “Unspecific FC” in 16%, “Spurious FC” in 1.5%, and “No FC” in 3.1% ([Fig. 5d](#)). “Specific FC” in 15/15 scans was found in 2 datasets (Median = 12/15). The “Specific FC” category was also more evenly distributed relative to acquisition protocols and

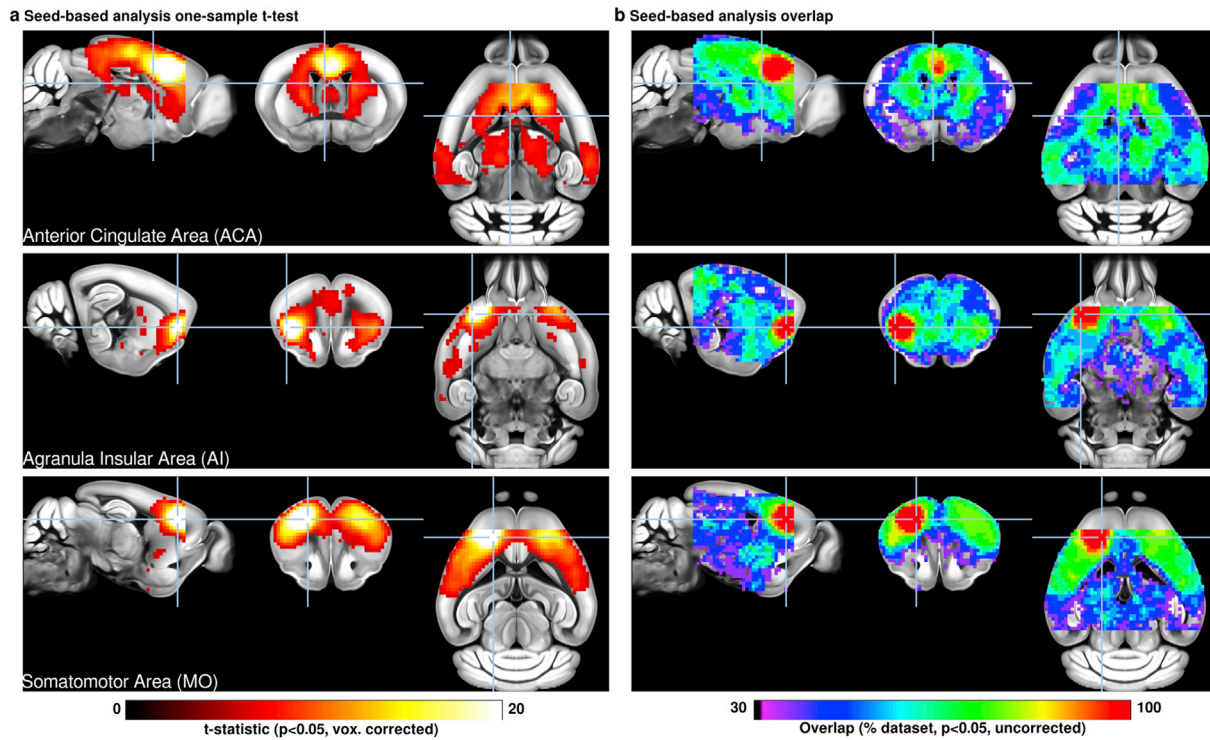


Fig. 3. Seed-based analyses (SBA) for 3 selected seeds positioned in the left hemisphere. One-sample *t*-test maps of individual maps reveal the full extent of SBA-derived resting-state networks in the mouse brain across 98/255 scans that presented “specific functional connectivity (FC)” following vascular + ventricle signal regression. FC relative to a seed located in the anterior cingulate area reveals the extent of the mouse default-mode network, including the dorsal caudoputamen, dorsal thalamus, and peri-hippocampal areas. The seed in the insular area reveals significant FC in dorsal cingulate and amygdalar areas, corresponding to areas previously associated with the human salience network. Inter-hemispheric homotopic FC is found relative to the somato-motor seed, together with lateral striatal FC. Overlap maps, indicating the percentage of datasets presenting significant FC after applying one-sample *t*-tests ($p < 0.05$, uncorrected), reveal that 12/17 of datasets recapitulated the features stated above. Out of these, 5 were not considered to overlap specifically (Supplementary Fig. 8). Voxelwise corrected *t*-statistic for one-sample *t*-tests and overlap maps are shown as a colour-coded overlays on the AIBS reference template.

equipments: Field strength (4.7 T $N = 14/15$, 7 T $N = 89/120$, 9.4 T $N = 73/90$, 11.7 T $N = 25/30$, $X^2 = 4.01$, $df = 3$, $p\text{-value} = 0.25$), coil type (room-temperature $N = 88/105$, cryoprobe $N = 113/150$, $X^2 = 2.17$, $df = 1$, $p\text{-value} = 0.14$), breathing condition (free-breathing $N = 138/180$, ventilated $N = 63/75$, $X^2 = 1.29$, $df = 1$, $p\text{-value} = 0.25$), and sedation condition (awake $N = 13/15$, isoflurane/halothane $N = 65/90$, medetomidine $N = 55/75$, medetomidine + isoflurane $N = 68/75$, $X^2 = 10.56$, $df = 3$, $p\text{-value} = 0.014$). Importantly, statistical inference revealed that significant within-component FC could be established in 17/17 datasets for all 14 components (Fig. 5c, Supplementary Fig. 11, Supplementary Fig. 12). This suggests that network-specific inferences can be probed in all rsfMRI datasets, and that drICA is a powerful approach enabling FC detection in all datasets, including those that may not robustly exhibit distal connectivity patterns.

4. Discussion

The rodent rsfMRI research field has been growing over the past 10 years (Chuang and Nasrallah, 2017; Gozzi and Schwarz, 2016; Hoyer et al., 2014; Jonckers et al., 2015, 2013; Pan et al., 2015). Fast-paced development of this field has yielded many exciting results, yet the comparability of these findings remains unclear. The results presented here indicate that, despite major differences in cross-site equipment, scan conditions, and sedation protocols, mouse rsfMRI networks converge toward spatially defined motifs encompassing previously described neuroanatomical systems of the mouse brain. Importantly, we also highlight the possibility of using rsfMRI to probe distributed network systems of high translational relevance, including a rodent DMN, salience network, and latero-cortical network. While not reliably identified in all datasets and scan conditions, these large-scale networks were found to

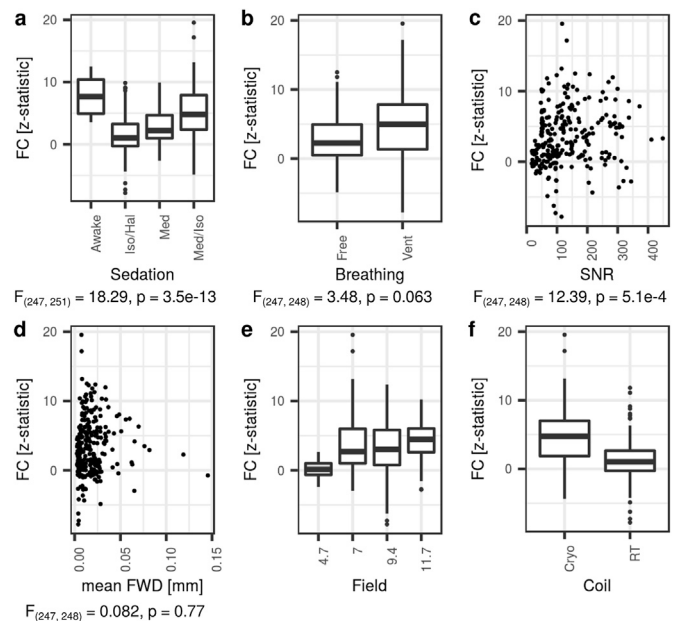


Fig. 4. Functional connectivity (FC) in the retrosplenial cortex relative to a seed located in the anterior cingulate area, as a function of acquisition parameters. A statistically significant association was determined between sedation effect and FC (a, $F_{(247, 251)} = 18.29$, $p = 3.5e-13$) and between SNR and FC (c, $F_{(247, 248)} = 12.39$, $p = 5.1e-4$). Neither breathing condition nor motion effects were significant with FC (b, d). Due to limitations in the representation of each level within a factor, coil design (e) and magnetic field (f) were omitted from the final statistical model. Free = free-breathing, Vent = mechanically ventilated, Cryo = cryoprobe, RT = room-temperature.

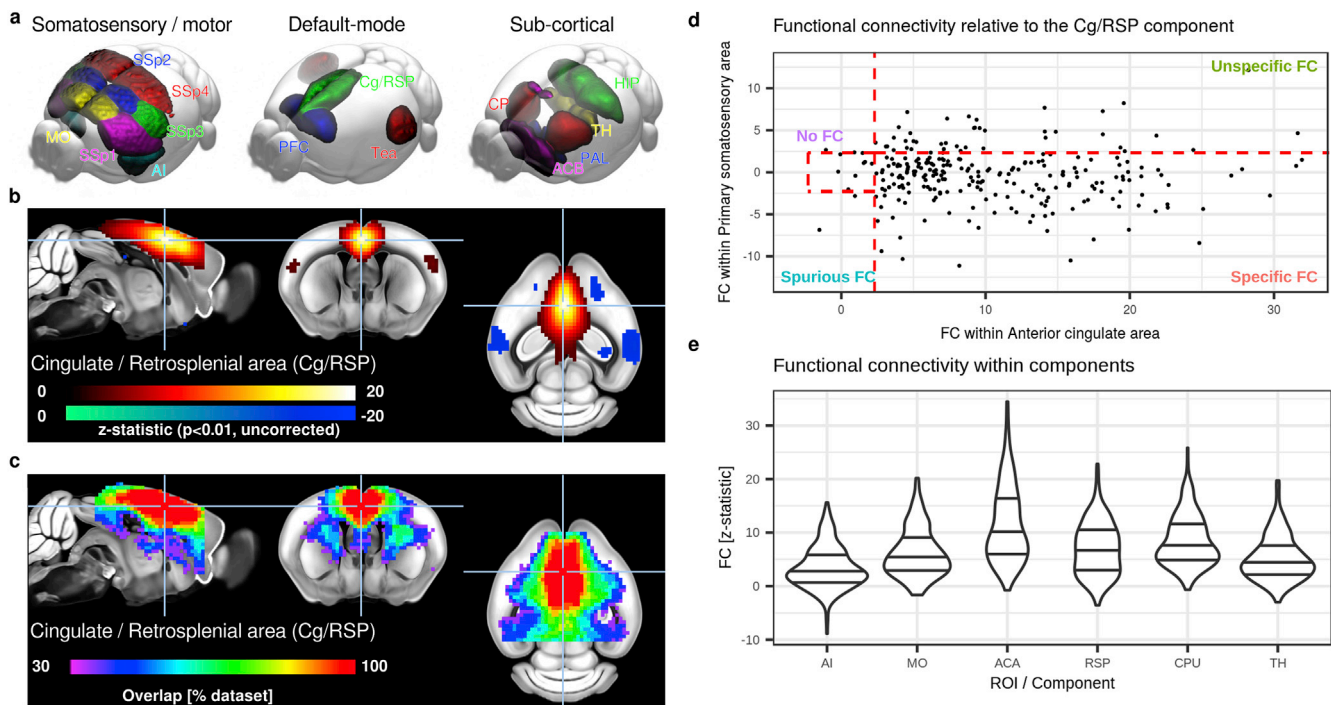


Fig. 5. Group-level independent component analysis (ICA) estimated across 98/255 “specific functional connectivity (FC)” scans reveals canonical mouse components (a). All components presented a marked bilateral organisation. Nine components were found to overlap principally with the isocortex including regions attributed to latero-cortical, salience, and DMN networks by seed-based analyses, three components overlapped with the striatum, one with the hippocampal areas, and one with the thalamus. Detailed representations of the cingulate/retrosplenial area component (Cg/RSP b). One-sample t-tests within datasets indicate that 100% of datasets presented significant FC ($p < 0.05$, uncorrected) within the Cg/RSP component (c). Remaining components are presented in [Supplementary Figs. 9 and 10](#). Overlap maps for the remaining components are presented in [Supplementary Figs. 11 and 12](#). FC relative to Cg/RSP is found specifically in the anterior cingulate area but not in the primary somatosensory in 79% of the individual scans following dual regression (d). FC strength distribution across 255 scans within selected components relative to ROIs defined in [Supplementary Fig. 1a](#) (e). Line intervals indicate 25th, 50th, and 75th percentiles. AI = insular area, MO = somato-motor area, SSp = primary somatosensory area, PFC = prefrontal cortex, Cg/RSP = cingulate + retrosplenial area, Tea = temporal associative area, CP = caudoputamen, ACB = nucleus accumbens, PAL = pallidum, HIP = hippocampal region, TH = thalamus.

colocalize within the well-delineated boundaries in the majority of scans and datasets, recapitulating previous descriptions in rodents ([Gozzi and Schwarz, 2016; Lu et al., 2012; Sforzini et al., 2014; Stafford et al., 2014](#)), monkeys ([Hutchison and Everling, 2012](#)), and humans ([Buckner et al., 2008](#)).

Interestingly, most (12/17) of the datasets converged toward spatially defined common RSNs when distal FC relative to a seed location was assessed. When the analysis was restricted to local connectivity, i.e. parameter estimates confined within the pre-defined networks, all (17/17) datasets converged. These results indicate that group-level, or second-level inferences, might be assessed irrespective of acquisition protocol or animal handling procedures using robust analysis strategies. At the subject level, “specific FC” relative to the DMN was found in 98/255 of the scans, indicating that first-level inference on distal FC is within reach in some, but not all datasets. Sedation and equipment performance leading to increased SNR were the major factors associated with both FC sensitivity and specificity, together with breathing conditions. Awake animals presented overall higher FC, however, datasets acquired with medetomidine + isoflurane combination together with mechanical ventilation were associated with greater specificity within elements of the DMN. Importantly, the results converged irrespective of sedation or awake protocols. This underlines that all datasets should be examined with the same criteria to further enhance results comparability. Hence, the set of standards provided here (e.g. spatial maps and FC parameter distributions), will allow for the calibration of future multi-centre projects and assist in designing meta-analysis and replication studies, the gold standards in evidence-based research.

In addition to acquisition procedures, the adoption of analysis standards must be encouraged. An MRI template ([Dorr et al., 2008](#))

transformed into the AIBS standard space provides a common space that extends beyond animal MRI studies, including the seamless implementation of AIBS resources ([Bergmann et al., 2016; Grandjean et al., 2017b; Oh et al., 2014; Richiardi et al., 2015; Stafford et al., 2014](#)). Moreover, analysis based on robust methods ([Zuo and Xing, 2014](#)), such as drICA ([Filippini et al., 2009](#)), together with considerations for statistical analysis ([Eklund et al., 2016](#)), and the sharing of datasets on online repositories ([Nichols et al., 2017](#)) provide a comprehensive evidence-based roadmap to improve the comparability of acquisitions carried out between centres and enhance the robustness and reproducibility of future results. In particular, all the datasets analysed in the context of this study have been made fully available and therefore will provide references for scientists developing customized rsfMRI protocols.

Several major limitations in this study should be acknowledged. First and foremost, the lack of consensus quality assurance parameters for the estimation of FC led us to devise a strategy to examine FC specificity. Human studies often use test-retest reliability method to assess protocol stability and reproducibility ([Zuo and Xing, 2014](#)), however, such metrics require duplicated acquisitions not presently available. Moreover, test-retest reliability might be biased in low-FC datasets, where the absence of FC is a reproducible feature. Because this study combined a set of existing scans, factors were not entirely orthogonal and it was not possible to model potentially relevant effects affecting FC metrics, such as specific sequence parameters (e.g. number of volumes), as well as biologically relevant factors including sex, age, and mouse strain. Additionally, the analysis was based on a fixed pre-processing pipeline. Different pipelines, beyond nuisance regression, have not been compared. Hence, different pre-processing step may favour specific acquisitions, e.g. adapted bandpass filters for anaesthesia protocols

(Grandjean et al., 2014a). The advent of standardized open-source pipelines dedicated to rodents, comparable to that found in humans (Esteban et al., 2019), may overcome this limitation in the future. Finally, the lack of distal FC in some datasets could not be attributed to specific animal handling protocols or equipment performance. This indicates that additional experimental factors not considered here might be better predictors in estimating this particular kind of FC. For example, the implementation of procedures to control the arterial level of carbon dioxide may be critical to prevent hypercapnic conditions, a feature that is associated with reduced FC connectivity (Biswal et al., 1997) and that is often observed in freely-breathing anaesthetized rodents. Despite these limitations, the work presented here is likely to enhance the true scientific value of mouse rsfMRI by establishing standards. With these, the field is set to meet its goals toward the establishment and understanding of the cellular and molecular mechanisms of large-scale brain functional reorganisation in the healthy and diseased brain.

Author contributions

JG designed the study. Every author contributed to data acquisition. JG, CC and AG carried out the analysis. Every author participated in the preparation of the manuscript.

Declaration of competing interest

A.M.L. has received consultant fees from Blueprint Partnership, Boehringer Ingelheim, Daimler und Benz Stiftung, Elsevier, F. Hoffmann-La Roche, ICARE Schizophrenia, K. G. Jebsen Foundation, L.E.K. Consulting, Lundbeck International Foundation (LINF), R. Adamczak, Roche Pharma, Science Foundation, Synapsis Foundation–Alzheimer Research Switzerland, and System Analytics and has received lectures including travel fees from Boehringer Ingelheim, Fama Public Relations, Institut d'investigacions Biomèdiques August Pi i Sunyer (IDIBAPS), Janssen-Cilag, Klinikum Christophsbad, Göppingen, Lilly Deutschland, Luzerner Psychiatrie, LVR Klinikum Düsseldorf, LWL Psychiatrie Verbund Westfalen-Lippe, Otsuka Pharmaceuticals, Reunions i Ciencia S. L., Spanish Society of Psychiatry, Südwestrundfunk Fernsehen, Stern TV, and Vitos Klinikum Kurhessen.

Acknowledgements

This work was supported by the Singapore Bioimaging Consortium (SBIC), A*STAR, Singapore. AG acknowledges funding from the Simons Foundation (SFARI 314688 and 400101), the Brain and Behavior Foundation (2017 NARSAD independent Investigator Grant) and the European Research Council (ERC, G.A. 802371). This work was also supported by the JSPS KAKENHI Grant Number 16K07032 to NT, 16K10233 to NY, and 18K18375 to CS, by Brain/MINDS, the Strategic Research Program for Brain Sciences (SRPBS) from the Ministry of Education, Culture, Sports, Science, and Technology of Japan (MEXT) and Japan Agency for Medical Research and Development (AMED) to NT and HO, by AMED under Grant Number JP19dm0307007h0002 and JP19dm0307008h0002 to NY, JP19dm0307026h0002 to CS, and 17dm0107066h to IA, by COI program by Japan Science and Technology Agency (JST) to IA, and by ERATO JPMJER1801 by JST to NY. It was further supported as part of the Excellence Cluster 'BrainLinks-BrainTools' by the German Research Foundation, grant EXC1086. AH acknowledges funding from the German BMBF (NeuroImpa, 01EC1403C and NeuroRad 02NUK034D). MD acknowledges funding from France-Alzheimer Association, Plan Alzheimer Foundation and the French Public Investment Bank's "ROMANE" program. This work was also supported by the Fund for Scientific Research Flanders (FWO) (grant agreements G057615N and 12S4815N - AvL), the Stichting Alzheimer Onderzoek (SAO-FRA, grant agreement 13026-AvL), the interdisciplinary PhD grant BOF DOCPRO 2014 - MV). NG acknowledges NEWMEDS project funded from the Innovative Medicine Initiative Joint Undertaking under Grant

Agreement no.115008 of which resources are composed of European Federation of Pharmaceutical Industries and Associations (EFPIA) in-kind contribution and financial contribution from the European Union's Seventh Framework Programme (FP7/2007-2013); as well as funding from the German Research Foundation (Deutsche Forschungsgemeinschaft): DFG SA 1869/15-1 and DFG GA 2109/2-1. The authors would like to thank Itamar Kahn, Eyal Bergmann and Daniel Gutierrez-Barragan for critically reading the manuscript.

Appendix A. Supplementary data

Supplementary data to this article can be found online at <https://doi.org/10.1016/j.neuroimage.2019.116278>.

References

- Avants, B.B., Tustison, N.J., Song, G., Cook, P.A., Klein, A., Gee, J.C., 2011. A reproducible evaluation of ANTs similarity metric performance in brain image registration. *Neuroimage* 54, 2033–2044. <https://doi.org/10.1016/j.neuroimage.2010.09.025>.
- Avants, B.B., Tustison, N.J., Stauffer, M., Song, G., Wu, B., Gee, J.C., 2014. The Insight ToolKit image registration framework. *Front. Neuroinf.* 8, 44. <https://doi.org/10.3389/fninf.2014.00044>.
- Azevedo, F.A.C., Carvalho, L.R.B., Grinberg, L.T., Farfel, J.M., Ferretti, R.E.L., Leite, R.E.P., Jacob Filho, W., Lent, R., Herculano-Houzel, S., 2009. Equal numbers of neuronal and nonneuronal cells make the human brain an isometrically scaled-up primate brain. *J. Comp. Neurol.* 513, 532–541. <https://doi.org/10.1002/cne.21974>.
- Becerra, L., Pendse, G., Chang, P.-C., Bishop, J., Borsook, D., 2011. Robust reproducible resting state networks in the awake rodent brain. *PLoS One* 6. <https://doi.org/10.1371/journal.pone.0025701> e25701.
- Belloy, M.E., Naeyaert, M., Abbas, A., Shah, D., Vanreusel, V., van Audekerke, J., Keilholz, S.D., Keliris, G.A., Van der Linden, A., Verhoye, M., 2018a. Dynamic resting state fMRI analysis in mice reveals a set of Quasi-Periodic Patterns and illustrates their relationship with the global signal. *Neuroimage* 180, 463–484. <https://doi.org/10.1016/j.neuroimage.2018.01.075>.
- Belloy, M.E., Shah, D., Abbas, A., Kashyap, A., Roßner, S., Van der Linden, A., Keilholz, S.D., Keliris, G.A., Verhoye, M., 2018b. Quasi-periodic patterns of neural activity improve classification of Alzheimer's disease in mice. *Sci. Rep.* 8, 10024. <https://doi.org/10.1038/s41598-018-28237-9>.
- Bergmann, E., Zur, G., Bershady, G., Kahn, I., 2016. The organization of mouse and human cortico-hippocampal networks estimated by intrinsic functional connectivity. *Cerebr. Cortex* 26, 4497–4512. <https://doi.org/10.1093/cercor/bhw327>.
- Bertero, A., Liska, A., Pagani, M., Parolisi, R., Masferrer, M.E., Gritti, M., Pedrazzoli, M., Galbusera, A., Sarica, A., Cerasa, A., Buffelli, M., Tonini, R., Buffo, A., Gross, C., Pasqualetti, M., Gozzi, A., 2018. Autism-associated 16p11.2 microdeletion impairs prefrontal functional connectivity in mouse and human. *Brain* 141, 2055–2065. <https://doi.org/10.1093/brain/awy111>.
- Biswal, B., Hudetz, A.G., Yetkin, F.Z., Haughton, V.M., Hyde, J.S., 1997. Hypercapnia reversibly suppresses low-frequency fluctuations in the human motor cortex during rest using echo-planar MRI. *J. Cerebr. Blood Flow Metab.* 17, 301–308. <https://doi.org/10.1097/00004647-199703000-00007>.
- Biswal, B., Yetkin, F.Z., Haughton, V.M., Hyde, J.S., 1995. Functional connectivity in the motor cortex of resting human brain using echo-planar MRI. *Magn. Reson. Med.* 34, 537–541. <https://doi.org/10.1002/mrm.1910340409>.
- Biswal, B., Mennes, M., Zuo, X.-N., Gohel, S., Kelly, C., Smith, S.M., Beckmann, C.F., Adelstein, J.S., Buckner, R.L., Colcombe, S., Dogonowski, A.-M., Ernst, M., Fair, D., Hampson, M., Hoptman, M.J., Hyde, J.S., Kiviniemi, V.J., Kötter, R., Li, S.-J., Lin, C.-P., Milham, M.P., 2010. Toward discovery science of human brain function. *Proc. Natl. Acad. Sci. U.S.A.* 107, 4734–4739. <https://doi.org/10.1073/pnas.0911855107>.
- Buckner, R.L., Andrews-Hanna, J.R., Schacter, D.L., 2008. The brain's default network: anatomy, function, and relevance to disease. *Ann. N. Y. Acad. Sci.* 1124, 1–38. <https://doi.org/10.1196/annals.1440.011>.
- Buehlmann, D., Grandjean, J., Xandry, J., Rudin, M., 2018. Longitudinal resting-state functional magnetic resonance imaging in a mouse model of metastatic bone cancer reveals distinct functional reorganizations along a developing chronic pain state. *Pain* 159, 719–727. <https://doi.org/10.1097/j.pain.0000000000001148>.
- Bukhari, Q., Schroeter, A., Cole, D.M., Rudin, M., 2017. Resting state fMRI in mice reveals anesthesia specific signatures of brain functional networks and their interactions. *Front. Neural Circuits* 11, 5. <https://doi.org/10.3389/fncir.2017.00005>.
- Bukhari, Q., Schroeter, A., Rudin, M., 2018. Increasing isoflurane dose reduces homotopic correlation and functional segregation of brain networks in mice as revealed by resting-state fMRI. *Sci. Rep.* 8, 10591. <https://doi.org/10.1038/s41598-018-28766-3>.
- Charbogne, P., Gardon, O., Martín-García, E., Keyworth, H.L., Matsui, A., Mechling, A.E., Bienert, T., Nasseef, T., Robé, A., Moquin, L., Darq, E., Ben Hamida, S., Robledo, P., Matifas, A., Befort, K., Gavériaux-Ruff, C., Harsan, L.-A., von Elverfeldt, D., Hennig, J., Gratton, A., Kieffer, B.L., 2017. Mu opioid receptors in gamma-aminobutyric acidergic forebrain neurons moderate motivation for heroin and palatable food. *Biol. Psychiatry* 81, 778–788. <https://doi.org/10.1016/j.biopsych.2016.12.022>.

- Chuang, K.-H., Nasrallah, F.A., 2017. Functional networks and network perturbations in rodents. *Neuroimage* 163, 419–436. <https://doi.org/10.1016/j.neuroimage.2017.09.038>.
- Cox, R.W., 1996. AFNI: software for analysis and visualization of functional magnetic resonance neuroimages. *Comput. Biomed. Res.* 29, 162–173. <https://doi.org/10.1006/cbmr.1996.0014>.
- DeSimone, J.C., Febo, M., Shukla, P., Ofori, E., Colon-Perez, L.M., Li, Y., Vaillancourt, D.E., 2016. In vivo imaging reveals impaired connectivity across cortical and subcortical networks in a mouse model of DYT1 dystonia. *Neurobiol. Dis.* 95, 35–45. <https://doi.org/10.1016/j.nbd.2016.07.005>.
- Dorr, A.E., Lerch, J.P., Spring, S., Kabani, N., Henkelman, R.M., 2008. High resolution three-dimensional brain atlas using an average magnetic resonance image of 40 adult C57Bl/6J mice. *Neuroimage* 42, 60–69. <https://doi.org/10.1016/j.neuroimage.2008.03.037>.
- Eklund, A., Nichols, T.E., Knutsson, H., 2016. Cluster failure: why fMRI inferences for spatial extent have inflated false-positive rates. *Proc. Natl. Acad. Sci. U.S.A.* 113, 7900–7905. <https://doi.org/10.1073/pnas.1602413113>.
- Errico, F., D'Argenio, V., Sforzini, F., Iasevoli, F., Squillace, M., Guerri, G., Napolitano, F., Angrisano, T., Di Maio, A., Keller, S., Vitucci, D., Galbusera, A., Chiariotti, L., Bertolino, A., de Bartolomeis, A., Salvatore, F., Gozzi, A., Usiello, A., 2015. A role for D-aspartate oxidase in schizophrenia and in schizophrenia-related symptoms induced by phencyclidine in mice. *Transl. Psychiatry* 5, e512. <https://doi.org/10.1038/tp.2015.2>.
- Esteban, O., Markiewicz, C.J., Blair, R.W., Moodie, C.A., Isik, A.I., Erramuzpe, A., Kent, J.D., Goncalves, M., DuPre, E., Snyder, M., Oya, H., Ghosh, S.S., Wright, J., Durme, J., Poldrack, R.A., Gorgolewski, K.J., 2019. fMRIPrep: a robust preprocessing pipeline for functional MRI. *Nat. Methods* 16, 111–116. <https://doi.org/10.1038/s41592-018-0235-4>.
- Filippini, N., MacIntosh, B.J., Hough, M.G., Goodwin, G.M., Frisoni, G.B., Smith, S.M., Matthews, P.M., Beckmann, C.F., Mackay, C.E., 2009. Distinct patterns of brain activity in young carriers of the APOE-epsilon4 allele. *Proc. Natl. Acad. Sci. U.S.A.* 106, 7209–7214. <https://doi.org/10.1073/pnas.0811879106>.
- Fox, M.D., Raichle, M.E., 2007. Spontaneous fluctuations in brain activity observed with functional magnetic resonance imaging. *Nat. Rev. Neurosci.* 8, 700–711. <https://doi.org/10.1038/nrn2201>.
- Fox, M.D., Snyder, A.Z., Vincent, J.L., Corbetta, M., Van Essen, D.C., Raichle, M.E., 2005. The human brain is intrinsically organized into dynamic, anticorrelated functional networks. *Proc. Natl. Acad. Sci. U.S.A.* 102, 9673–9678. <https://doi.org/10.1073/pnas.0504136102>.
- Friston, K.J., 2011. Functional and effective connectivity: a review. *Brain Connect.* 1, 13–36. <https://doi.org/10.1089/brain.2011.0008>.
- Gass, N., Weber-Fahr, W., Sartorius, A., Becker, R., Didriksen, M., Stensbøl, T.B., Bastlund, J.F., Meyer-Lindenberg, A., Schwarz, A.J., 2016. An acetylcholine alpha7 positive allosteric modulator rescues a schizophrenia-associated brain endophenotype in the 15q13.3 microdeletion, encompassing CHRNA7. *Eur. Neuropsychopharmacol.* 26, 1150–1160. <https://doi.org/10.1016/j.euroneuro.2016.03.013>.
- Gozzi, A., Schwarz, A.J., 2016. Large-scale functional connectivity networks in the rodent brain. *Neuroimage* 127, 496–509. <https://doi.org/10.1016/j.neuroimage.2015.12.017>.
- Grandjean, J., Azzinnari, D., Seuwen, A., Sigrist, H., Seifritz, E., Pryce, C.R., Rudin, M., 2016a. Chronic psychosocial stress in mice leads to changes in brain functional connectivity and metabolite levels comparable to human depression. *Neuroimage* 142, 544–552. <https://doi.org/10.1016/j.neuroimage.2016.08.013>.
- Grandjean, J., Derungs, R., Kulic, L., Welt, T., Henkelman, M., Nitsch, R.M., Rudin, M., 2016b. Complex interplay between brain function and structure during cerebral amyloidosis in APP transgenic mouse strains revealed by multi-parametric MRI comparison. *Neuroimage* 134, 1–11. <https://doi.org/10.1016/j.neuroimage.2016.03.042>.
- Grandjean, J., Preti, M.G., Bolton, T.A.W., Buerge, M., Seifritz, E., Pryce, C.R., Van De Ville, D., Rudin, M., 2017a. Dynamic reorganization of intrinsic functional networks in the mouse brain. *Neuroimage* 152, 497–508. <https://doi.org/10.1016/j.neuroimage.2017.03.026>.
- Grandjean, J., Schroeter, A., Batata, I., Rudin, M., 2014a. Optimization of anesthesia protocol for resting-state fMRI in mice based on differential effects of anesthetics on functional connectivity patterns. *Neuroimage* 102 (2), 838–847. <https://doi.org/10.1016/j.neuroimage.2014.08.043>. Pt.
- Grandjean, J., Schroeter, A., He, P., Tanadini, M., Keist, R., Krstic, D., Konietzko, U., Klohs, J., Nitsch, R.M., Rudin, M., 2014b. Early alterations in functional connectivity and white matter structure in a transgenic mouse model of cerebral amyloidosis. *J. Neurosci.* 34, 13780–13789. <https://doi.org/10.1523/JNEUROSCI.4762-13.2014>.
- Grandjean, J., Zerbi, V., Balsters, J.H., Wenderoth, N., Rudin, M., 2017b. Structural basis of large-scale functional connectivity in the mouse. *J. Neurosci.* 37, 8092–8101. <https://doi.org/10.1523/JNEUROSCI.0438-17.2017>.
- Greicius, M., 2008. Resting-state functional connectivity in neuropsychiatric disorders. *Curr. Opin. Neurol.* 21, 424–430. <https://doi.org/10.1097/WCO.0b013e328306f2c5>.
- Guilfoyle, D.N., Gerum, S.V., Sanchez, J.L., Balla, A., Sershen, H., Javitt, D.C., Hoptman, M.J., 2013. Functional connectivity fMRI in mouse brain at 7T using isoflurane. *J. Neurosci. Methods* 214, 144–148. <https://doi.org/10.1016/j.jneumeth.2013.01.019>.
- Gutierrez-Barragan, D., Basson, M.A., Panzeri, S., Gozzi, A., 2019. Intraslow state fluctuations govern spontaneous fMRI network dynamics. *Curr. Biol.* 29, 2295–2306. <https://doi.org/10.1016/j.cub.2019.06.017> e5.
- Haberl, M.G., Zerbi, V., Veltien, A., Ginger, M., Heerschap, A., Frick, A., 2015. Structural-functional connectivity deficits of neocortical circuits in the Fmr1 (-/y) mouse model of autism. *Sci. Adv.* 1. <https://doi.org/10.1126/sciadv.1500775> e1500775.
- Hoyer, C., Gass, N., Weber-Fahr, W., Sartorius, A., 2014. Advantages and challenges of small animal magnetic resonance imaging as a translational tool. *Neuropsychobiology* 69, 187–201. <https://doi.org/10.1159/000360859>.
- Hübner, N.S., Mechling, A.E., Lee, H.-L., Reiser, M., Bienert, T., Hennig, J., von Elverfeldt, D., Harsan, L.-A., 2017. The connectomics of brain demyelination: functional and structural patterns in the cuprizone mouse model. *Neuroimage* 146, 1–18. <https://doi.org/10.1016/j.neuroimage.2016.11.008>.
- Hutchison, R.M., Everling, S., 2012. Monkey in the middle: why non-human primates are needed to bridge the gap in resting-state investigations. *Front. Neuroanat.* 6, 29. <https://doi.org/10.3389/fnana.2012.00029>.
- Jonckers, E., Delgado y Palacios, R., Shah, D., Guglielmetti, C., Verhoye, M., Van der Linden, A., 2014. Different anesthesia regimes modulate the functional connectivity outcome in mice. *Magn. Reson. Med.* 72, 1103–1112. <https://doi.org/10.1002/mrm.24990>.
- Jonckers, E., Shah, D., Hamaide, J., Verhoye, M., Van der Linden, A., 2015. The power of using functional fMRI on small rodents to study brain pharmacology and disease. *Front. Pharmacol.* 6, 231. <https://doi.org/10.3389/fphar.2015.00231>.
- Jonckers, E., Van Audekerke, J., De Visscher, G., Van der Linden, A., Verhoye, M., 2011. Functional connectivity fMRI of the rodent brain: comparison of functional connectivity networks in rat and mouse. *PLoS One* 6. <https://doi.org/10.1371/journal.pone.0018876> e18876.
- Jonckers, E., Van der Linden, A., Verhoye, M., 2013. Functional magnetic resonance imaging in rodents: an unique tool to study in vivo pharmacologic neuroimaging. *Curr. Opin. Pharmacol.* 13, 813–820. <https://doi.org/10.1016/j.coph.2013.06.008>.
- Jovicich, J., Minati, L., Marziconi, M., Marchitelli, R., Sala-Llonch, R., Barrés-Faz, D., Arnold, J., Benninghoff, J., Fiedler, U., Roccatagliata, L., Picco, A., Nobili, F., Blin, O., Bombois, S., Lopes, R., Bordet, R., Sein, J., Ranjeva, J.-P., Didic, M., Gros-Dagnac, H., PharmaCog Consortium, 2016. Longitudinal reproducibility of default-mode network connectivity in healthy elderly participants: a multicentric resting-state fMRI study. *Neuroimage* 124, 442–454. <https://doi.org/10.1016/j.neuroimage.2015.07.010>.
- Kalthoff, D., Po, C., Wiedermann, D., Hoehn, M., 2013. Reliability and spatial specificity of rat brain sensorimotor functional connectivity networks are superior under sedation compared with general anesthesia. *NMR Biomed.* 26, 638–650. <https://doi.org/10.1002/nbm.2908>.
- Komaki, Y., Hikishima, K., Shibata, S., Konomi, T., Seki, F., Yamada, M., Miyasaka, N., Fujiyoshi, K., Okano, H.J., Nakamura, M., Okano, H., 2016. Functional brain mapping using specific sensory-circuit stimulation and a theoretical graph network analysis in mice with neuropathic allodynia. *Sci. Rep.* 6, 37802. <https://doi.org/10.1038/srep37802>.
- Lein, E.S., Hawrylycz, M.J., Ao, N., Ayres, M., Bensinger, A., Bernard, A., Boe, A.F., Boguski, M.S., Brockway, K.S., Byrnes, E.J., Chen, L., Chen, L., Chen, T.-M., Chin, M.C., Chong, J., Crook, B.E., Czaplinski, A., Dang, C.N., Datta, S., Dee, N.R., Jones, A.R., 2007. Genome-wide atlas of gene expression in the adult mouse brain. *Nature* 445, 168–176. <https://doi.org/10.1038/nature05453>.
- Liska, A., Bertero, A., Gomolka, R., Sabbioni, M., Galbusera, A., Barsotti, N., Panzeri, S., Scattoni, M.L., Pasqualetti, M., Gozzi, A., 2018. Homozygous loss of autism-risk gene CNTNAP2 results in reduced local and long-range prefrontal functional connectivity. *Cereb. Cortex* 28, 1141–1153. <https://doi.org/10.1093/cercor/bhx022>.
- Liska, A., Galbusera, A., Schwarz, A.J., Gozzi, A., 2015. Functional connectivity hubs of the mouse brain. *Neuroimage* 115, 281–291. <https://doi.org/10.1016/j.neuroimage.2015.04.033>.
- Liska, A., Gozzi, A., 2016. Can mouse imaging studies bring order to autism connectivity chaos? *Front. Neurosci.* 10, 484. <https://doi.org/10.3389/fnins.2016.00484>.
- Li, Q., Li, G., Wu, D., Lu, H., Hou, Z., Ross, C.A., Yang, Y., Zhang, J., Duan, W., 2017. Resting-state functional MRI reveals altered brain connectivity and its correlation with motor dysfunction in a mouse model of Huntington's disease. *Sci. Rep.* 7, 16742. <https://doi.org/10.1038/s41598-017-17026-5>.
- Lu, H., Zou, Q., Gu, H., Raichle, M.E., Stein, E.A., Yang, Y., 2012. Rat brains also have a default mode network. *Proc. Natl. Acad. Sci. U.S.A.* 109, 3979–3984. <https://doi.org/10.1073/pnas.1200506109>.
- Mechling, A.E., Arefin, T., Lee, H.-L., Bienert, T., Reiser, M., Ben Hamida, S., Darcq, E., Ehrlich, A., Gaveriaux-Ruff, C., Parent, M.J., Rosa-Neto, P., Hennig, J., von Elverfeldt, D., Kieffer, B.L., Harsan, L.-A., 2016. Deletion of the mu opioid receptor gene in mice reshapes the reward-aversion connectome. *Proc. Natl. Acad. Sci. U.S.A.* 113, 11603–11608. <https://doi.org/10.1073/pnas.1601640113>.
- Michetti, C., Caruso, A., Pagani, M., Sabbioni, M., Medrihan, L., David, G., Galbusera, A., Morini, M., Gozzi, A., Benfenati, F., Scattoni, M.L., 2017. The knockout of synapsin II in mice impairs social behavior and functional connectivity generating an ASD-like phenotype. *Cereb. Cortex* 27, 5014–5023. <https://doi.org/10.1093/cercor/bhx207>.
- Murphy, K., Birn, R.M., Bandettini, P.A., 2013. Resting-state fMRI confounds and cleanup. *Neuroimage* 80, 349–359. <https://doi.org/10.1016/j.neuroimage.2013.04.001>.
- Nichols, T.E., Das, S., Eickhoff, S.B., Evans, A.C., Glattard, T., Hanke, M., Kriegeskorde, N., Milham, M.P., Poldrack, R.A., Poline, J.-B., Proal, E., Thirion, B., Van Essen, D.C., White, T., Yeo, B.T.T., 2017. Best practices in data analysis and sharing in neuroimaging using MRI. *Nat. Neurosci.* 20, 299–303. <https://doi.org/10.1038/nn.4500>.
- Oguz, I., Zhang, H., Rumble, A., Sonka, M., 2014. RATS: rapid automatic tissue segmentation in rodent brain MRI. *J. Neurosci. Methods* 221, 175–182. <https://doi.org/10.1016/j.jneumeth.2013.09.021>.
- Oh, S.W., Harris, J.A., Ng, L., Winslow, B.T., Cui, N., Mihalas, S., Wang, Q., Lau, C., Kuan, L., Henry, A.M., Mortrud, M.T., Ouellette, B., Nguyen, T.N., Sorensen, S.A., Slaughterbeck, C.R., Wakeman, W., Li, Y., Feng, D., Ho, A., Nicholas, E., Zeng, H.,

2014. A mesoscale connectome of the mouse brain. *Nature* 508, 207–214. <https://doi.org/10.1038/nature13186>.
- Paasonen, J., Stenroos, P., Salo, R.A., Kiviniemi, V., Gröhn, O., 2018. Functional connectivity under six anesthesia protocols and the awake condition in rat brain. *Neuroimage* 172, 9–20. <https://doi.org/10.1016/j.neuroimage.2018.01.014>.
- Pan, W.-J., Billings, J.C.W., Grooms, J.K., Shakil, S., Keilholz, S.D., 2015. Considerations for resting state functional MRI and functional connectivity studies in rodents. *Front. Neurosci.* 9, 269. <https://doi.org/10.3389/fnins.2015.00269>.
- Popa, D., Popescu, A.T., Paré, D., 2009. Contrasting activity profile of two distributed cortical networks as a function of attentional demands. *J. Neurosci.* 29, 1191–1201. <https://doi.org/10.1523/JNEUROSCI.4867-08.2009>.
- Razoux, F., Baltes, C., Mueggler, T., Seuwen, A., Russig, H., Mansuy, I., Rudin, M., 2013. Functional MRI to assess alterations of functional networks in response to pharmacological or genetic manipulations of the serotonergic system in mice. *Neuroimage* 74, 326–336. <https://doi.org/10.1016/j.neuroimage.2013.02.031>.
- Richiardi, J., Altmann, A., Milazzo, A.-C., Chang, C., Chakravarty, M.M., Banaschewski, T., Barker, G.J., Bokke, A.L.W., Bromberg, U., Büchel, C., Conrod, P., Fauth-Bühler, M., Flor, H., Frouin, V., Gallinat, J., Garavan, H., Gowland, P., Heinz, A., Lemaitre, H., Mann, K.F., 2015. IMAGEN consortium, 2015. BRAIN NETWORKS. Correlated gene expression supports synchronous activity in brain networks. *Science* 348, 1241–1244. <https://doi.org/10.1126/science.1255905>.
- Rorden, C., Karnath, H.-O., Bonilha, L., 2007. Improving lesion-symptom mapping. *J. Cogn. Neurosci.* 19, 1081–1088. <https://doi.org/10.1162/jocn.2007.19.7.1081>.
- Schroeter, A., Grandjean, J., Schlegel, F., Saab, B.J., Rudin, M., 2017. Contributions of structural connectivity and cerebrovascular parameters to functional magnetic resonance imaging signals in mice at rest and during sensory paw stimulation. *J. Cereb. Blood Flow Metab.* 37, 2368–2382. <https://doi.org/10.1177/0271678X16666292>.
- Sethi, S.S., Zerbi, V., Wenderoth, N., Fornito, A., Fulcher, B.D., 2017. Structural connectome topology relates to regional BOLD signal dynamics in the mouse brain. *Chaos* 27. <https://doi.org/10.1063/1.4979281>, 047405.
- Sforzini, F., Bertero, A., Dodero, L., David, G., Galbusera, A., Scattoni, M.L., Pasqualetti, M., Gozzi, A., 2016. Altered functional connectivity networks in allocasol and socially impaired BTBR mice. *Brain Struct. Funct.* 221, 941–954. <https://doi.org/10.1007/s00429-014-0948-9>.
- Sforzini, F., Schwarz, A.J., Galbusera, A., Bifone, A., Gozzi, A., 2014. Distributed BOLD and CBV-weighted resting-state networks in the mouse brain. *Neuroimage* 87, 403–415. <https://doi.org/10.1016/j.neuroimage.2013.09.050>.
- Shah, D., Blockx, I., Guns, P.-J., De Deyn, P.P., Van Dam, D., Jonckers, E., Delgado Y Palacios, R., Verhoye, M., Van der Linden, A., 2015. Acute modulation of the cholinergic system in the mouse brain detected by pharmacological resting-state functional MRI. *Neuroimage* 109, 151–159. <https://doi.org/10.1016/j.neuroimage.2015.01.009>.
- Shah, D., Blockx, I., Keliris, G.A., Kara, F., Jonckers, E., Verhoye, M., Van der Linden, A., 2016a. Cholinergic and serotonergic modulations differentially affect large-scale functional networks in the mouse brain. *Brain Struct. Funct.* 221, 3067–3079. <https://doi.org/10.1007/s00429-015-1087-7>.
- Shah, D., Deleye, S., Verhoye, M., Staelens, S., Van der Linden, A., 2016b. Resting-state functional MRI and [18F]-FDG PET demonstrate differences in neuronal activity between commonly used mouse strains. *Neuroimage* 125, 571–577. <https://doi.org/10.1016/j.neuroimage.2015.10.073>.
- Shah, D., Jonckers, E., Praet, J., Vanhoutte, G., Delgado Y Palacios, R., Bigot, C., D'Souza, D.V., Verhoye, M., Van der Linden, A., 2013. Resting state fMRI reveals diminished functional connectivity in a mouse model of amyloidosis. *PLoS One* 8. <https://doi.org/10.1371/journal.pone.0084241> e84241.
- Shah, D., Praet, J., Latif Hernandez, A., Höfling, C., Anckaerts, C., Bard, F., Morawski, M., Detrez, J.R., Prinsen, E., Villa, A., De Vos, W.H., Maggi, A., D'Hooge, R., Balschun, D., Rossner, S., Verhoye, M., Van der Linden, A., 2016c. Early pathologic amyloid induces hypersynchrony of BOLD resting-state networks in transgenic mice and provides an early therapeutic window before amyloid plaque deposition. *Alzheimers Dement.* 12, 964–976. <https://doi.org/10.1016/j.jalz.2016.03.010>.
- Stafford, J.M., Jarrett, B.R., Miranda-Dominguez, O., Mills, B.D., Cain, N., Mihalas, S., Lahvis, G.P., Lattal, K.M., Mitchell, S.H., David, S.V., Fryer, J.D., Nigg, J.T., Fair, D.A., 2014. Large-scale topology and the default mode network in the mouse connectome. *Proc. Natl. Acad. Sci. U.S.A.* 111, 18745–18750. <https://doi.org/10.1073/pnas.1404346111>.
- Upadhyay, J., Baker, S.J., Chandran, P., Miller, L., Lee, Y., Marek, G.J., Sakoglu, U., Chin, C.-L., Luo, F., Fox, G.B., Day, M., 2011. Default-mode-like network activation in awake rodents. *PLoS One* 6. <https://doi.org/10.1371/journal.pone.0027839> e27839.
- Wiesmann, M., Zerbi, V., Jansen, D., Haast, R., Lütjohann, D., Broersen, L.M., Heerschap, A., Kiliaan, A.J., 2016. A dietary treatment improves cerebral blood flow and brain connectivity in aging apoE4 mice. *Neural Plast.* 2016, 6846721. <https://doi.org/10.1155/2016/6846721>.
- Wu, T., Grandjean, J., Bosshard, S.C., Rudin, M., Reutens, D., Jiang, T., 2017. Altered regional connectivity reflecting effects of different anaesthesia protocols in the mouse brain. *Neuroimage* 149, 190–199. <https://doi.org/10.1016/j.neuroimage.2017.01.074>.
- Yoshida, K., Mimura, Y., Ishihara, R., Nishida, H., Komaki, Y., Minakuchi, T., Tsurugizawa, T., Mimura, M., Okano, H., Tanaka, K.F., Takata, N., 2016. Physiological effects of a habituation procedure for functional MRI in awake mice using a cryogenic radiofrequency probe. *J. Neurosci. Methods* 274, 38–48. <https://doi.org/10.1016/j.jneumeth.2016.09.013>.
- Zerbi, V., Grandjean, J., Rudin, M., Wenderoth, N., 2015. Mapping the mouse brain with rs-fMRI: an optimized pipeline for functional network identification. *Neuroimage* 123, 11–21. <https://doi.org/10.1016/j.neuroimage.2015.07.090>.
- Zerbi, V., Ielacqua, G.D., Markicevic, M., Haberl, M.G., Ellisman, M.H., A-Bhaskaran, A., Frick, A., Rudin, M., Wenderoth, N., 2018. Dysfunctional autism risk genes cause circuit-specific connectivity deficits with distinct developmental trajectories. *Cerebr. Cortex* 28, 2495–2506. <https://doi.org/10.1093/cercor/bhy046>.
- Zerbi, V., Wiesmann, M., Emmerzaal, T.L., Jansen, D., Van Beek, M., Mutsaers, M.P.C., Beckmann, C.F., Heerschap, A., Kiliaan, A.J., 2014. Resting-state functional connectivity changes in aging apoE4 and apoE-KO mice. *J. Neurosci.* 34, 13963–13975. <https://doi.org/10.1523/JNEUROSCI.0684-14.2014>.
- Zhan, Y., Paolicelli, R.C., Sforzini, F., Weinhard, L., Bolasco, G., Pagani, F., Vysotski, A.L., Bifone, A., Gozzi, A., Ragozzino, D., Gross, C.T., 2014. Deficient neuron-microglia signaling results in impaired functional brain connectivity and social behavior. *Nat. Neurosci.* 17, 400–406. <https://doi.org/10.1038/nn.3641>.
- Zuo, X.-N., Xing, X.-X., 2014. Test-retest reliabilities of resting-state fMRI measurements in human brain functional connectomics: a systems neuroscience perspective. *Neurosci. Biobehav. Rev.* 45, 100–118. <https://doi.org/10.1016/j.neubiorev.2014.05.009>.